AD

AD-E403 287

Technical Report ARMET-TR-10001

# CRITICAL FLAW ESTIMATE AND FLAW ANALYSIS OF 81-mm M821A1 MORTAR PROJECTILE

J. Jablonski
J.A. Cordes
M. Hespos
D. Geissler
M. Carlini

June 2010

U.S. ARMY ARMAMENT RESEARCH, DEVELOPMENT AND ENGINEERING CENTER

Munitions Engineering Technology Center

Picatinny Arsenal, New Jersey

The views, opinions, and/or findings contained in this report are those of the author(s) and should not be construed as an official Department of the Army position, policy, or decision, unless so designated by other documentation.

The citation in this report of the names of commercial firms or commercially available products or services does not constitute official endorsement by or approval of the U.S. Government.

Destroy this report when no longer needed by any method that will prevent disclosure of its contents or reconstruction of the document. Do not return to the originator.

| REPORT DOCUMENTATION PAGE | | | *Form Approved OMB No. 0704-01-0188* |
|---|---|---|---|



| 1. REPORT DATE (DD-MM-YYYY) | 2. REPORT TYPE | 3. DATES COVERED (*From - To*) |
|---|---|---|
| June 2020 | Interim | June to September 2009 |

| 4. TITLE AND SUBTITLE | 5a. CONTRACT NUMBER |
|---|---|
| CRITICAL FLAW ESTIMATE AND FLAW ANALYSIS OF 81-mm M821A1 MORTAR PROJECTILE | 5b. GRANT NUMBER |
| | 5c. PROGRAM ELEMENT NUMBER |
| 6. AUTHORS | 5d. PROJECT NUMBER |
| J. Jablonski, J. A. Cordes, M. Hespos, D. Geissler, and M. Carlini | 5e. TASK NUMBER |
| | 5f. WORK UNIT NUMBER |

| 7. PERFORMING ORGANIZATION NAME(S) AND ADDRESS(ES) | 8. PERFORMING ORGANIZATION REPORT NUMBER |
|---|---|
| U.S. Army ARDEC, METC<br>Fuze & Precision Armaments Technology Directorate<br>(RDAR-MEF-E)<br>Picatinny Arsenal, NJ 07806-5000 | |
| 9. SPONSORING/MONITORING AGENCY NAME(S) AND ADDRESS(ES) | 10. SPONSOR/MONITOR'S ACRONYM(S) |
| U.S. Army ARDEC, ESIC<br>Knowledge & Process Management (RDAR-EIK)<br>Picatinny Arsenal, NJ 07806-5000 | 11. SPONSOR/MONITOR'S REPORT NUMBER(S)<br>Technical Report ARMET-TR-10001 |

12. DISTRIBUTION/AVAILABILITY STATEMENT

Approved for public release; distribution is unlimited.

13. SUPPLEMENTARY NOTES

14. ABSTRACT

Recent inspection of 81-mm mortar shells indicated the presence of flaws extending up to a third of the way through the wall thickness, as well as flaws internal to the shell body. Although no injuries have been recorded, this prompted an analysis of the mortar shell to determine what the critical flaw size is. Using the ABAQUS software, the mortar shell was analyzed with and without flaws to determine if the part would survive the loading of hydro testing and gun launch. The NASGRO software package was also used to find the critical flaw size for the shell. The critical flaw size was determined to be one fourth of the way through the wall thickness of the mortar body and was recommended as an inspection criterion for acceptance of 81-mm mortar shell parts.

15. SUBJECT TERMS

Finite element method ABAQUS NASGRO M821 Critical flaw estimate

| 16. SECURITY CLASSIFICATION OF: | | | 17. LIMITATION OF ABSTRACT | 18. NUMBER OF PAGES | 19a. NAME OF RESPONSIBLE PERSON |
|---|---|---|---|---|---|
| a. REPORT | b. ABSTRACT | c. THIS PAGE | | | J. Jablonski |
| U | U | U | SAR | | 19b. TELEPHONE NUMBER (Include area code) (973) 724-1384 |

## ACKNOWLEDGMENTS

The mortars team wishes to thank Dave G. Katz for his expertise and continued vigilance regarding the inspection for flaws and defects in production mortars.

## CONTENTS

## FIGURES

## FIGURES

## INTRODUCTION

The Army's 81-mm mortar is subjected to numerous tests to make sure that rounds are safe for gun-fire. The bodies are inspected after the steel parts are manufactured using non-destructive, ultrasound equipment. The mortar bodies are then sent to another plant, filled with explosive, and inspected again. Mortar bodies with flaws that exceed a critical size are not released to soldiers. This 81-mm mortar body has been in production for more than 20 yrs without a safety issue. There are no known cases of an 81-mm mortar causing damage to a gun or a soldier during gun-fire.

During a recent post loading x-ray inspection of an 81-mm mortar, a flaw was detected. The explosive fill was removed and the body was re-inspected. The flaw was still present. This is highly unusual as the bodies are ultrasonically inspected prior to being shipped to the loading facility. The body was returned to the U.S. Army Armament Research, Development and Engineering Center (ARDEC), Picatinny Arsenal, New Jersey for further evaluation. After receiving the 81-mm mortar body, it was returned to the production facility that produced it, where it was re-inspected with the regular production ultrasonic inspection equipment. An Army Non-Destructive Testing expert monitored this re-inspection process. The ultrasonic inspection equipment registered an above normal return signal in the area of the flaws, but the signal's magnitude was under the rejection level threshold. The body was then brought back to ARDEC for destructive metallurgical evaluation.

In metallurgical tests, the flaws appeared to extend to a depth of one third the wall thickness of the shell body (figs. 1 and 2). When the defect was first found, the original stress analysis was reviewed to determine how highly loaded this particular area of the body was. The hand analysis was not adequate to determine the likelihood that this defect would be significant enough to cause a failure, so the technical community sought to re-do the analysis with modern finite element analysis (FEA) techniques. In response, a FEA on an 81-mm mortar shell was completed to determine if the damage could result in a safety issue. The critical flaw size was also reviewed.

Photos this page show defect in longitudinal cross section. The defect occupies up to 1/3 of the body's wall thickness.

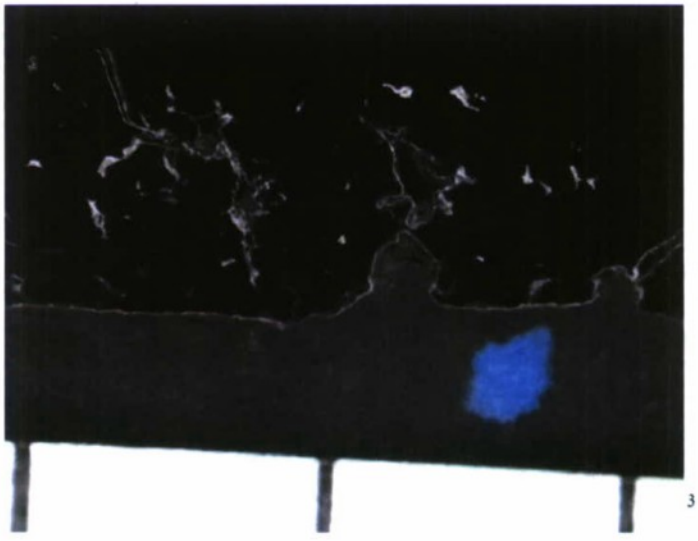

Figure 1
Damage in the wall of an 81-mm mortar [each dash is 2.5-mm (ref.1)]

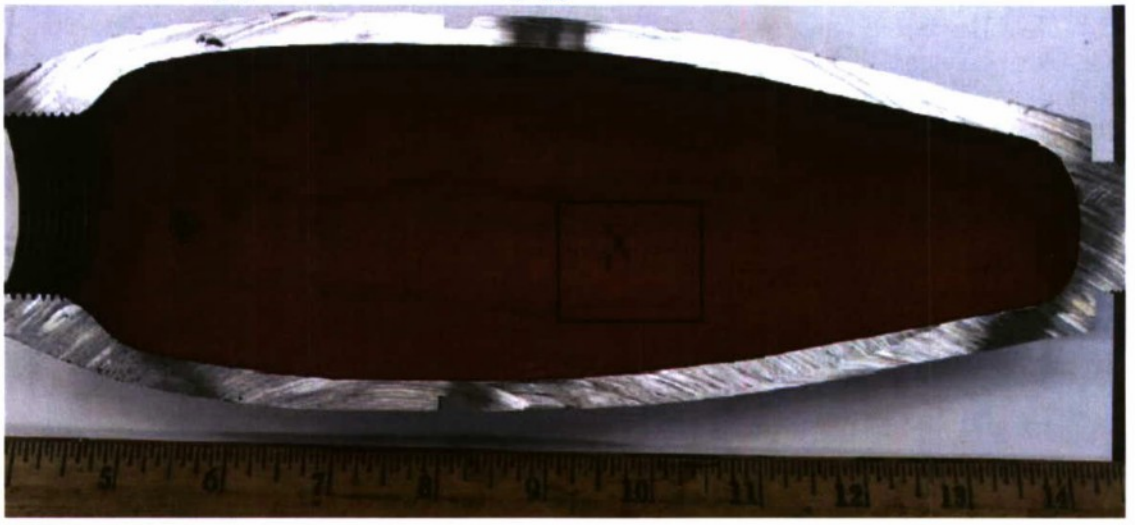

Figure 2
Location of defect, 81-mm mortar (ref. 1)

## METHOD

### Overview

The structural integrity of an 81-mm M821A1 mortar round with flaws on the inner surface and interior of the shell was evaluated. The analysis simulated hydrostatic testing and a dynamic gun-shot. Additionally, analyses were performed without a defect present to determine the critical flaw size of the shell body.

### General Method

The general-purposed finite element package ABAQUS 6.9-1 (ref. 2) was used for obtaining the required stress distributions for the analyses. In the flaw analysis, ABAQUS 6.9-1 was used to calculate the stress distribution around the flaws. In determining the critical flaw size, ABAQUS 6.9-1 was used to calculate the maximum hoop stress and its stress distribution through the shell wall. This data was then imported into NASGRO 5.0 (ref. 3) to calculate the critical flaw size.

### Modeling Assumptions

In the flaw analysis, balloting and blow-by were not considered. Rather, only structural analysis based on hydrostatic testing conditions and a pressure-time curve (simulating gun launch) was performed. Two pressure-time curves were used in the simulation. One pressure-time curve was not from an 81-mm mortar, but rather from a 60-mm mortar (ref. 4), as the maximum gun-launch pressure was known to be similar and represent a conservative upper bound. A second pressure-time curve was reconstructed from data on a zone 4 charge fired in an 81-mm mortar at 21°C (ref. 1).

It was assumed that a planar symmetry existed along the centerline of the M821A1 and so a half-model was used to simplify the computational requirements of the simulation. In the flaw analysis, this meant that a half-crack for the interior flaw was also used. The geometry of the internal flaw remained unaffected by the symmetry plane. In the assembly, the threads of the fuze were not modeled and tie constraints between the fuze and shell were used to simulate fastening. The fuze modeled was scaled from a 60-mm fuze as drawings for an 81-mm fuze were unavailable. In effect, the fuze was approximated and assumed to be representative of the actual structure. All contact for this model was assumed to be frictionless.

Material properties for the fuze, which is aluminum, were generalized since no particular alloy or data was provided. Additionally, the true material properties for Composition B were estimated and treated as linear-elastic.

## Geometry

The M821A1 assembly consists of three components with the part of interest being the M821A1 shell. The fuze and round composition were also incorporated into the assembly. Figure 3 shows the geometry. It was assumed that the shell was completely filled with composition B and additional components, such as the explosive train, were ignored. This was done because the purpose of the analysis was to focus on the shell. The explosives housed within it were irrelevant. The composition B was included to ensure that the round would not be simulated as hollow. For the flaw analysis, the shell was modeled with a defect on the interior surface. The flaw was dimensioned with a maximum depth of one third the wall thickness and a length that was twice the width. An internal flaw in the shell was incorporated approximately half-way through the shell with a depth of one fourth the wall thickness. The geometries of these flaws are representative of the observed defects in the M821A1 body, roughly (fig. 1).

Figure 3
Geometry of M821A1 projectile with flaws

## Material Models

The material properties used for the analysis are summarized in table 1. The shell body was modeled as HF-1 steel with assumed yield strength of 552 MPa (ref. 4). The material properties of the fuze and composition B were estimated and included for weight and stiffness. The fuze was assumed to be aluminum with a half-volume of 57.5-cm$^3$. The true properties of composition B have no appreciable impact on the simulation results.

Table 1
Summary of material properties

| Part | Material Properties | Notes |
|---|---|---|
| Shell | m = 1.085 kg<br>E = 207 GPa<br>v = 0.33<br>Yield strength = 552 MPa<br>Tensile strength = 1158 MPa<br>True plastic strain = 0.08 | Assumed material properties of HF-1 steel. |
| Fuze | m = 0.045 kg<br>E = 69 GPa | Generalized material properties of aluminum. |
| Composition B | m = 0.028 kg<br>E = 345 GPa<br>v = 0.33 | Given "dummy" properties for purposes of simulation. |

## Finite Element Mesh

A total of 111,201 hexahedral reduced integration mesh elements (C3D8R) with enhanced hour glass controls were used in the analysis. The overall geometry of the applied mesh can be seen in figure 4. Table 2 summarizes the number of elements used for each part. Refined meshes with a total of 17,516 elements were applied around the flaws to further improve the accuracy of the analysis. Approximately 25% of the elements used to model the shell were focused around the flaws. The mesh used for the interior flaw can be seen in figure 5. The mesh used for the internal flaw is shown in figure 6. A similar mesh to figure 4 was also used for the critical flaw size estimates. For critical flaw estimates, eight elements were used through the thickness to sufficiently represent the hoop and axial stress distributions.

Figure 4
Finite element mesh of the assembly

Table 2
Element summary

| Part | Elements |
|---|---|
| Shell<br>(Flaw internal)<br>(Flaw interior) | 74,266<br>(13,244)<br>(4,272) |
| Fuze | 21,834 |
| Composition B | 12,176 |
| **TOTAL** | **111,201** |

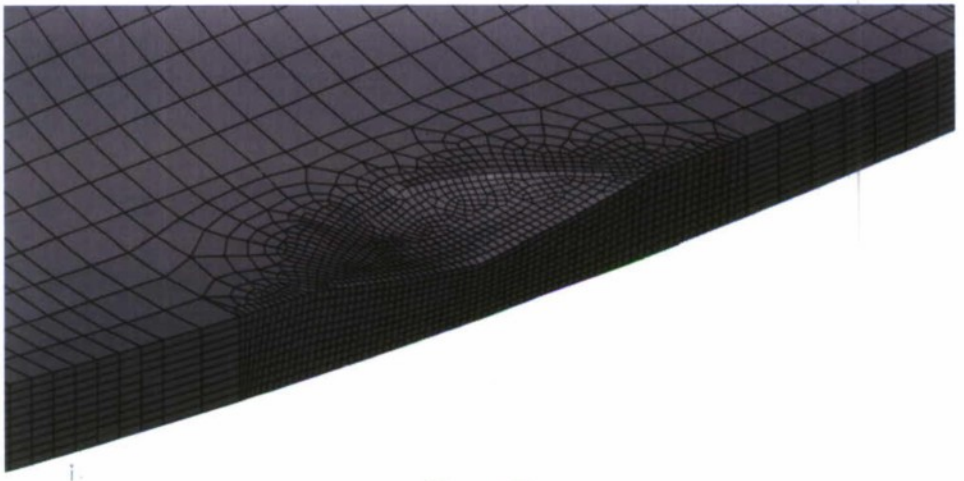

Figure 5
Detailed finite element mesh of interior flaw

Figure 6
Location and finite element mesh of internal flaw

## Load Cases

Two load cases were considered during the simulation. In the first case, the M821A1 shell was subjected to a hydrostatic test. In the latter case, the M821A1 assembly was subjected to a pressure-time curve simulating typical gun launch conditions. These loading cases were used to represent the total life-cycle of a round through testing and fielding.

To simulate hydrostatic testing, the inner surface of the M821A1 shell was subjected to a maximum loading of 67.2 MPa (fig. 7). The loading was applied using a smooth step curve increasing from zero pressure to maximum loading over 0.003 sec. Upon completion of this time interval, the loading was removed using a smooth step curve decreasing from maximum loading to zero pressure.

Figure 7
Hydrostatic test loads on the shell body

For the purpose of modeling gun launch conditions, a pressure-time curve was obtained from a 60-mm M821A1 launch. It was assumed that this pressure-time curve would be representative of maximum load conditions faced during an 81-mm launch, reflecting overpressure at gun launch. This loading was applied to the exterior of the M821A1 shell aft of the rotating band seat (fig. 8). Figure 9 shows a plot of the pressure-time curve used in the simulation. Additional analysis used a reconstructed pressure-time curve from a zone 4 charge fired at 21°C from an 81-mm mortar to more accurately simulate actual gun launch conditions (fig. 10).

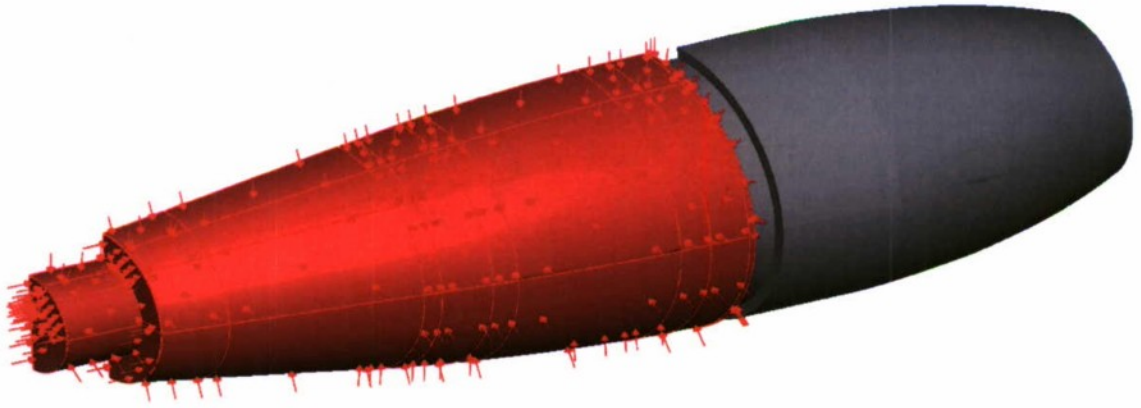

Figure 8
Gun loads on the shell body

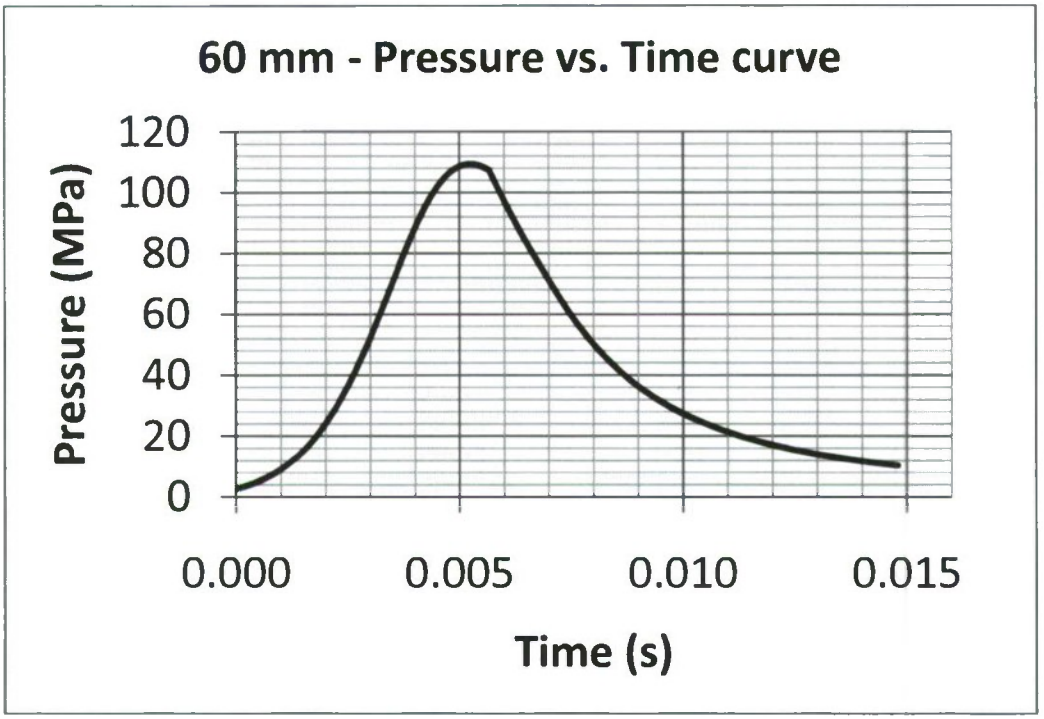


Figure 9
M821A1 overpressure curve estimated from a 60-mm mortar (ref. 4)

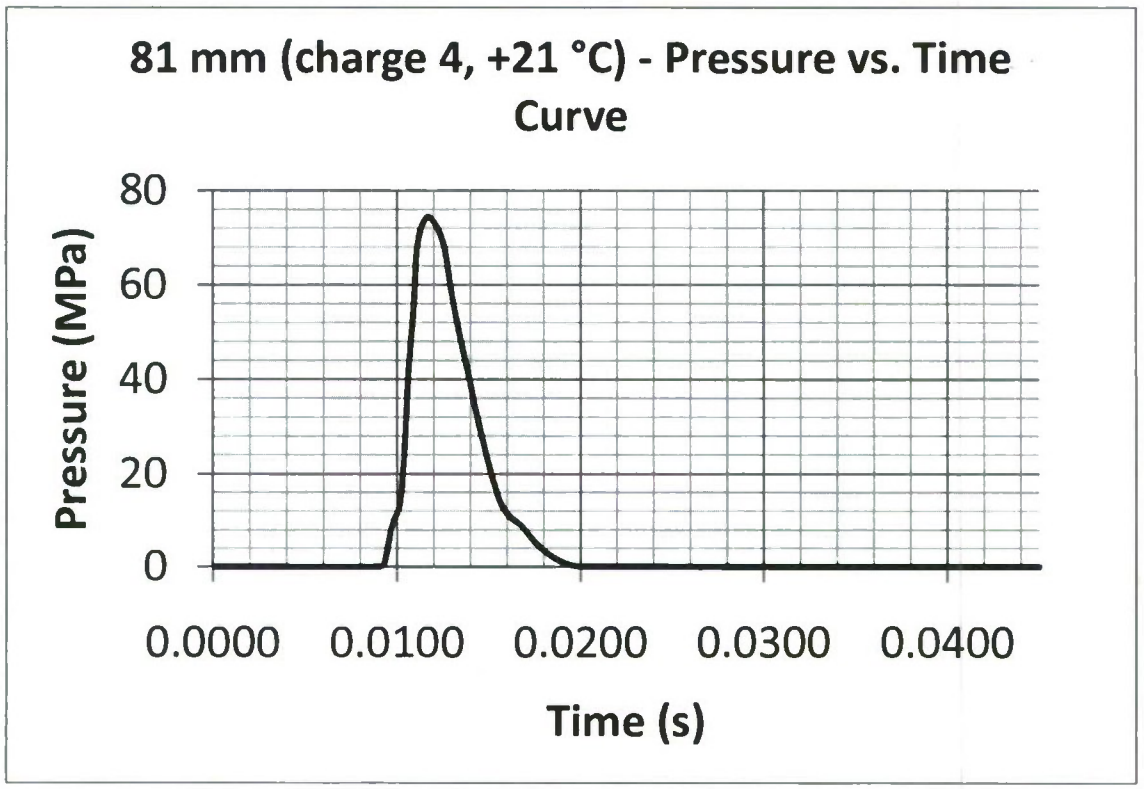


Figure 10
Reconstructed M821A1 pressure versus time curve

### Failure Criteria

The following failure criteria were used for the shell body of the M821A1 projectile (ref. 5):

- Plastic strain > % material elongation or
- Plastic strain > 1/4 net ligament or
- Equivalent von Mises stress > ultimate tensile strength

Technically, none of the failure criteria were met for the finite element analysis. However, because the incorporated flaw was greater than one fourth the net ligament, the part was already deemed to be a failure. In other words, although it was not likely that the shell body would catastrophically fail during operation, the flawed regions make it unsuitable for use.

## FLAW ANALYSIS

### Hydrostatic Testing - Interior Flaw

The maximum stresses during hydrostatic testing of the M821A1 shell occurred on the surface of the flaw. When a hydrostatic test was performed at a pressure of 67.2 MPa, there was a maximum resultant stress of 557 MPa, exceeding the yield strength of the material. A contour plot of the stress distribution around the flaw can be seen in figure 11. The region that yields was limited to the surface of the flaw. Figure 12 shows the stress distribution through the wall. The stress distribution, taken from the deepest point of the flaw, illustrates the limited yielding through the thickness of the wall.

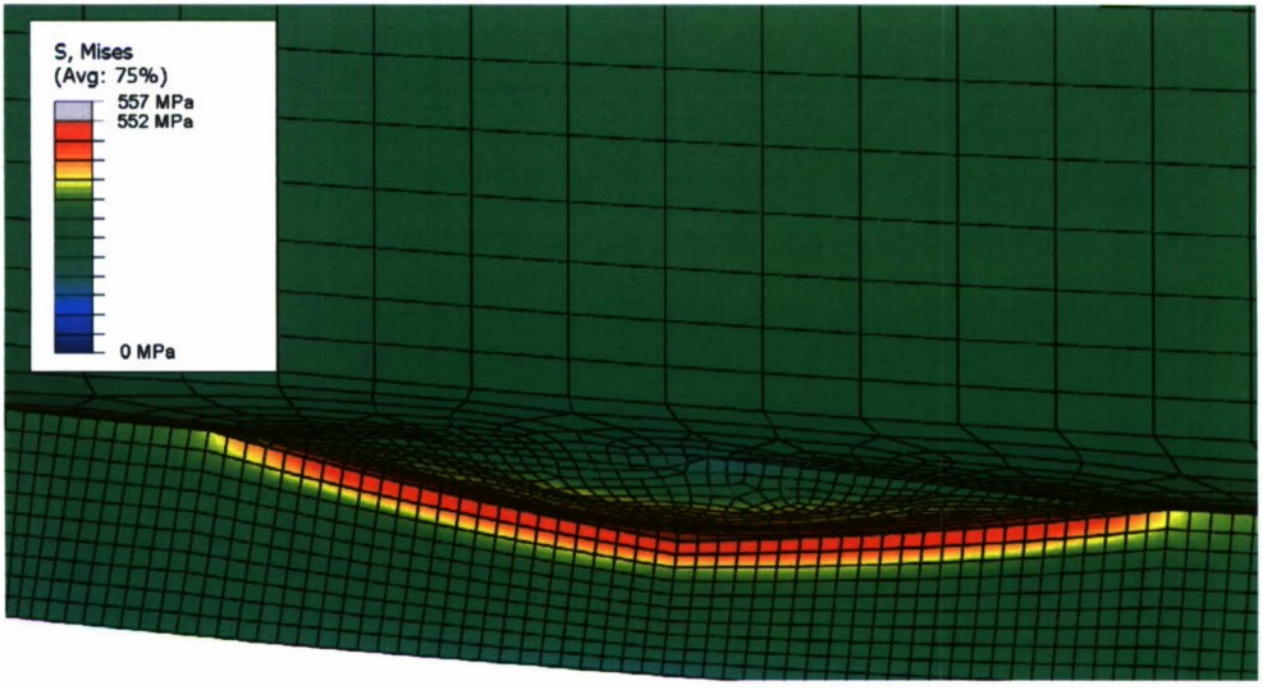


Figure 11
Peak equivalent von Mises stresses of interior flaw during hydrostatic testing

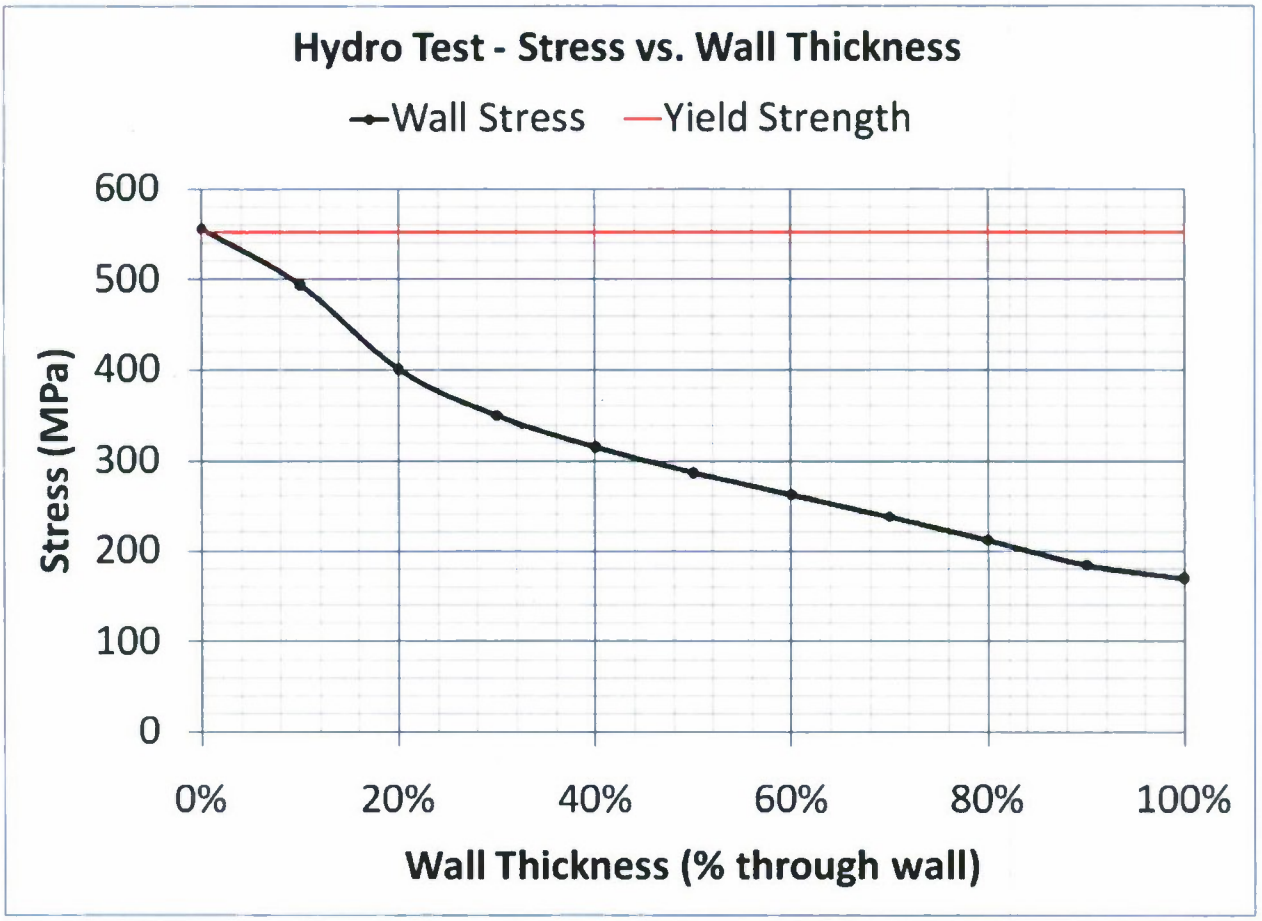


Figure 12
von Mises stress of interior flaw during hydrostatic testing

### Hydrostatic Testing - Internal Flaw

The maximum stress during hydrostatic testing of the interior flaw occurred on its surface. When a hydrostatic test was performed at a pressure of 67.2 MPa, there was a maximum resultant stress of 355 MPa. A contour plot of the stress distribution around the flaw can be seen in figure 13. The stress distribution through the interior flaw was well below the yield strength of the material (fig. 14).

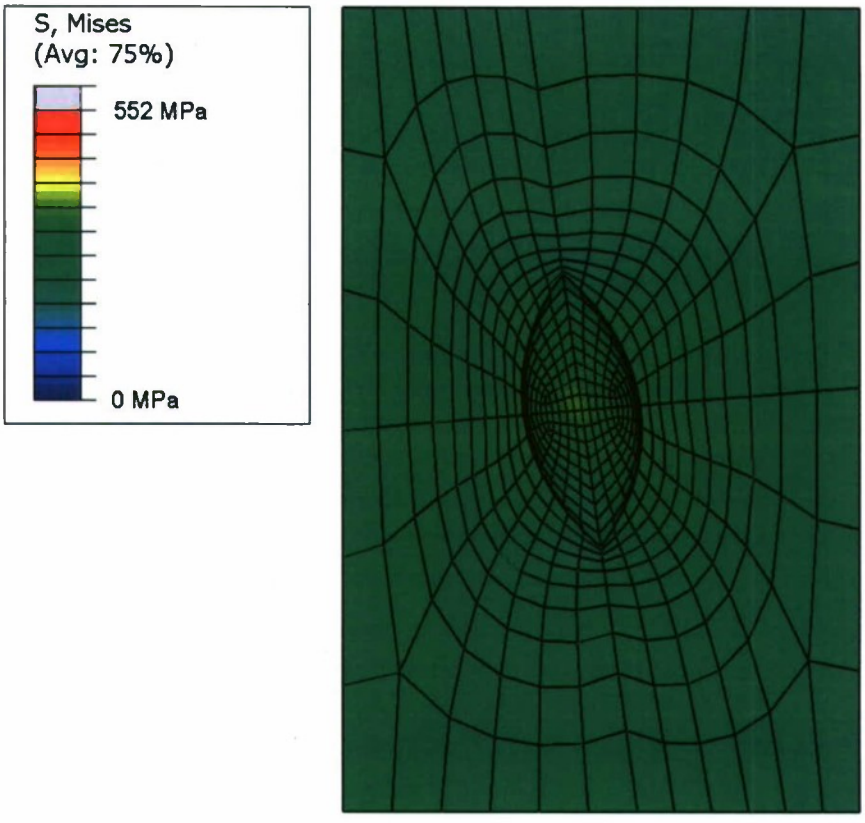


Figure 13
Peak equivalent von Mises stresses of internal flaw during hydrostatic testing

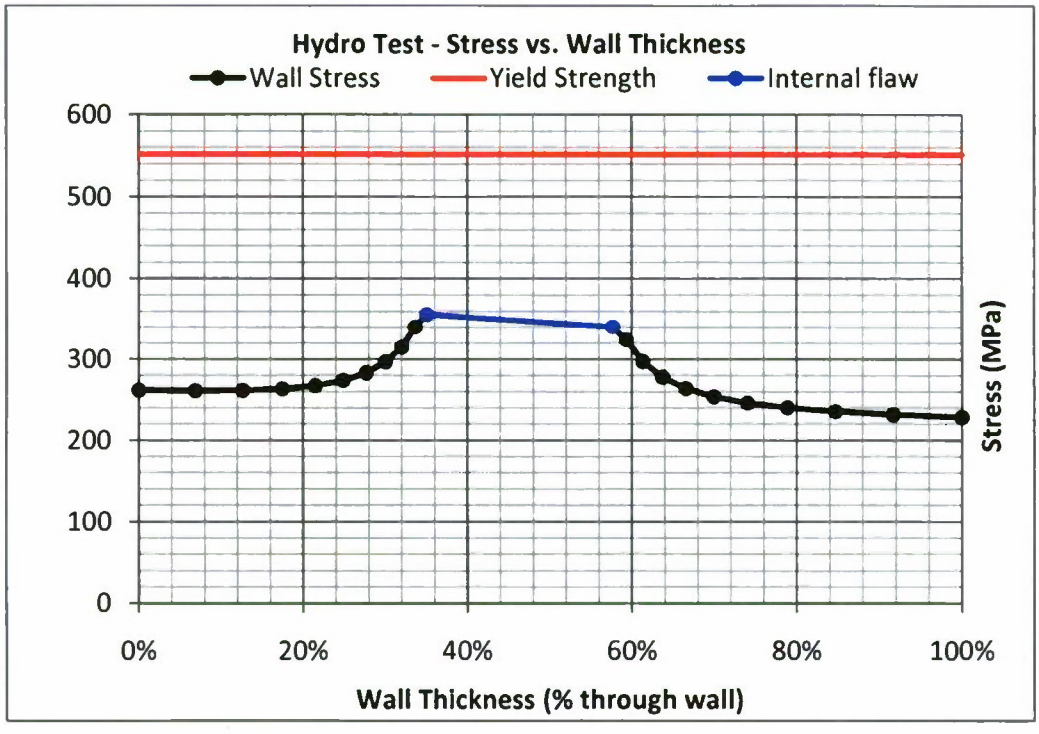


Figure 14
von Mises stress of internal flaw during hydrostatic testing along flaw hoop axis

## Gun Launch - Interior Flaw (Overpressure)

The maximum stresses during gun launch of the M821A1 shell occurred on the surface of the flaw. At this time (5.04 ms) there was a maximum resultant stress of 577 MPa, exceeding the yield strength of the material. A contour plot of the stress distribution around the flaw can be seen in figure 15. The wall yields through approximately 12% of its thickness. Figure 16 shows the stress distribution through the wall thickness. This distribution was used to determine the critical flaw size.

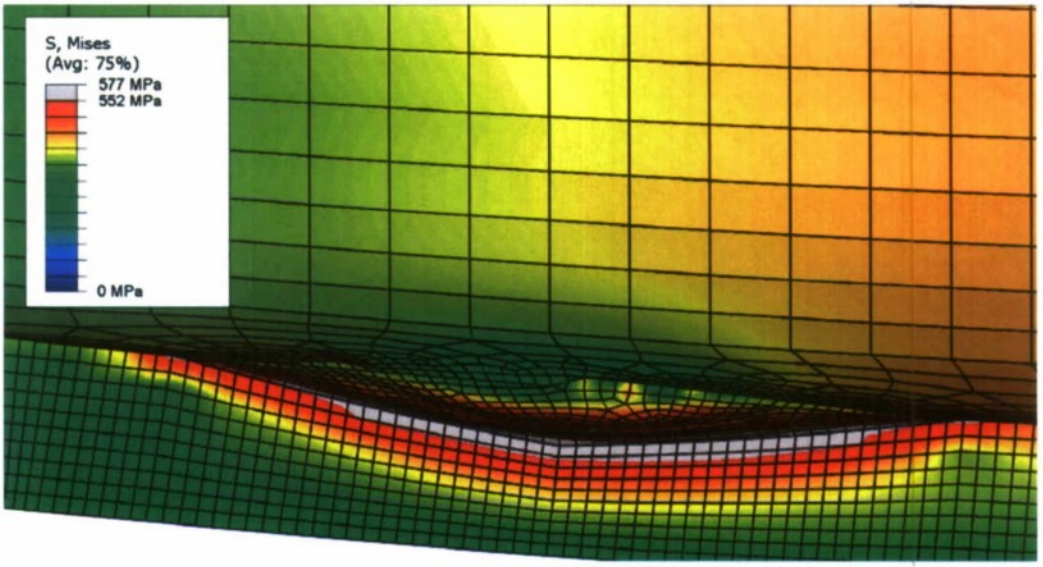


Figure 15
Peak equivalent von Mises stresses at interior flaw with overpressure

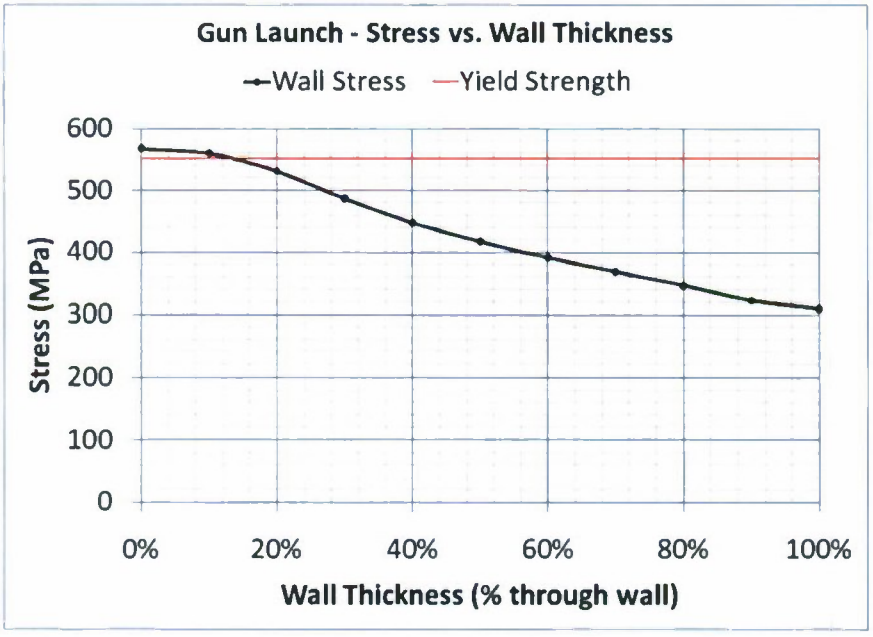


Figure 16
von Mises stress through the thinnest wall section of interior flaw with overpressure

Gun Launch - Interior Flaw (81-mm pressure-time curve)

The maximum stresses during gun launch of the M821A1 shell occurred on the surface of the flaw. At this time (11.7 ms), there was a maximum resultant stress of 398 MPa. A contour plot of the stress distribution around the flaw can be seen in figure 17. The stress distribution through the interior flaw was well below the yield strength of the material (fig. 18).

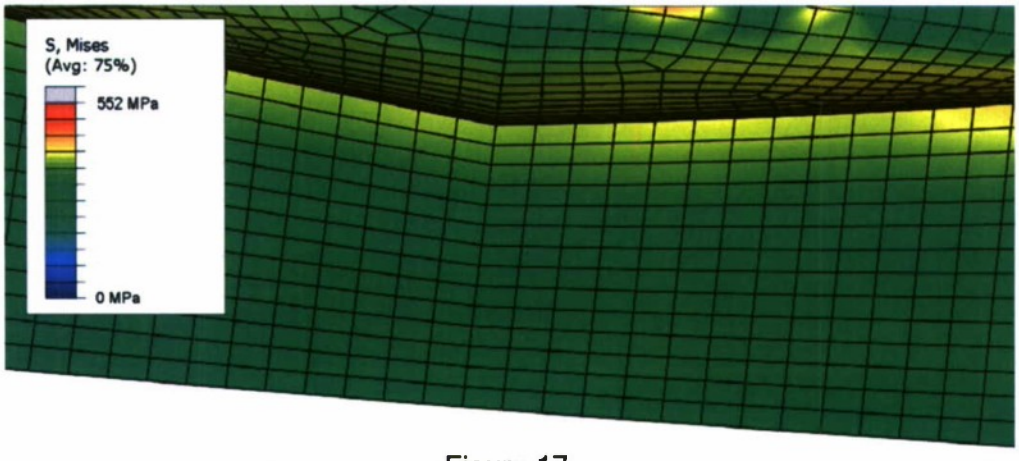


Figure 17
Peak equivalent von Mises stresses at interior flaw with 81-mm pressure-time curve

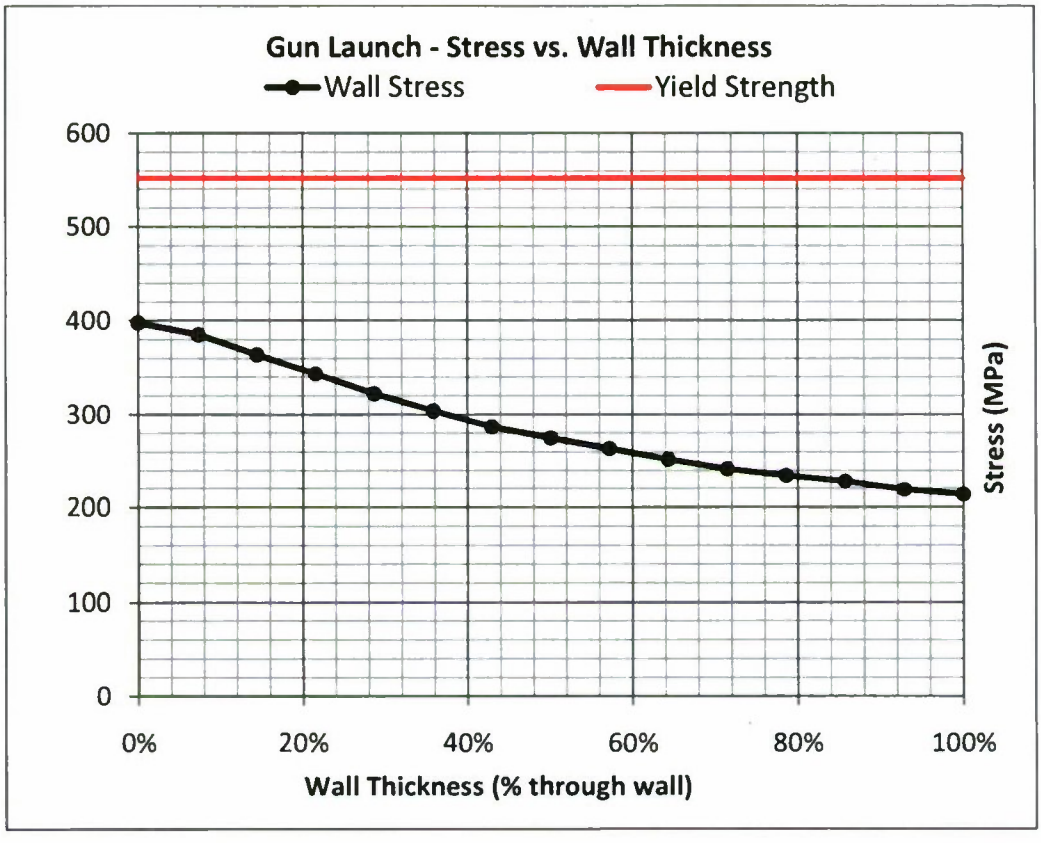


Figure 18
von Mises stress through the thinnest wall section of interior flaw with 81-mm pressure-time curve

Gun Launch - Internal Flaw (81-mm pressure-time curve)

The maximum stress during gun launch of the interior flaw occurred on its surface. At this time (11.7 ms) there was a maximum resultant stress of 270 MPa. A contour plot of the stress distribution around the flaw can be seen in figure 19. The stress distribution through the internal flaw was well below the yield strength of the material (fig. 20).

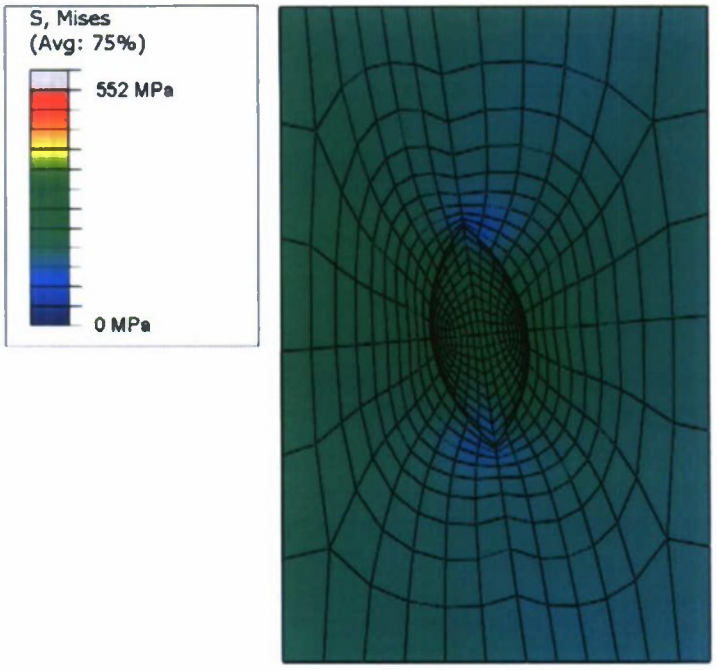


Figure 19
Peak equivalent von Mises stresses of internal flaw with 81-mm pressure-time curve
(This flaw is inside the shell wall.)

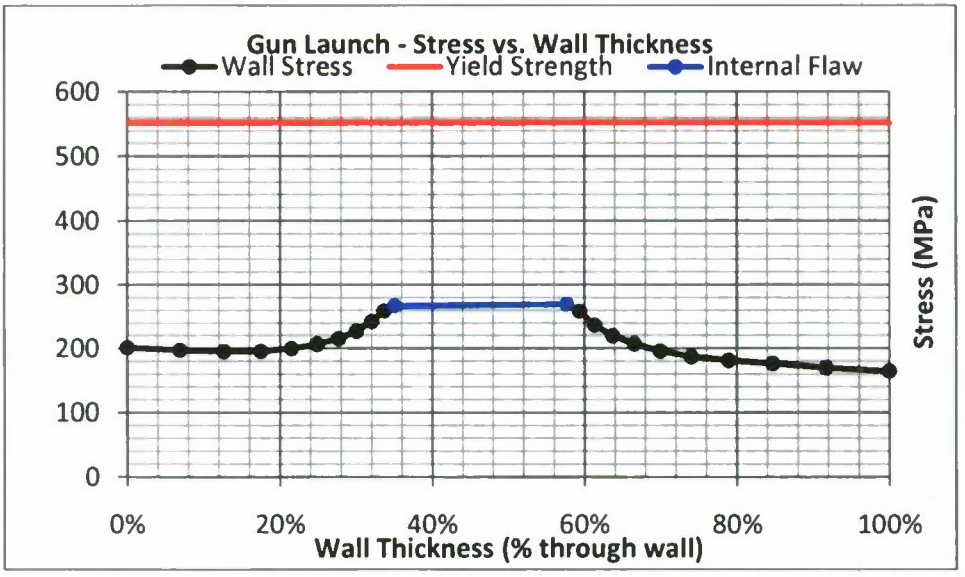


Figure 20
von Mises stress of internal flaw with 81-mm pressure-time curve along flaw hoop axis

## Additional Discussion

The results of the hydrostatic testing analysis indicated that some yielding occurred on the outer edge of the band seat. While historically there have been no associated failures related to this, it was important that this result be documented. According to the finite element model, a stress of 557 MPa was present on the exterior surface of the band seat. A contour plot of the von Mises stress distribution is shown in figure 21. The yielding through the band seat was limited to approximately 5% of the wall thickness, which is depicted in the stress distribution in figure 22.

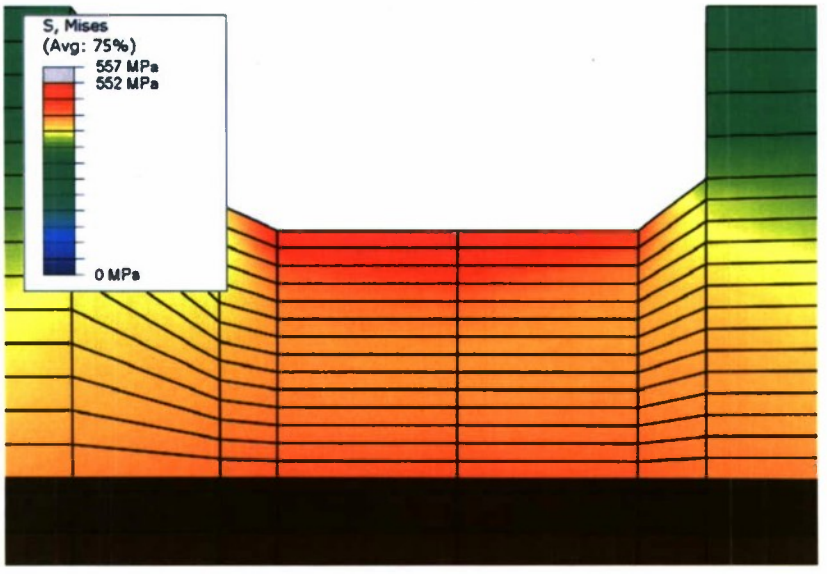


Figure 21
Peak equivalent von Mises stresses during hydrostatic testing at band seat

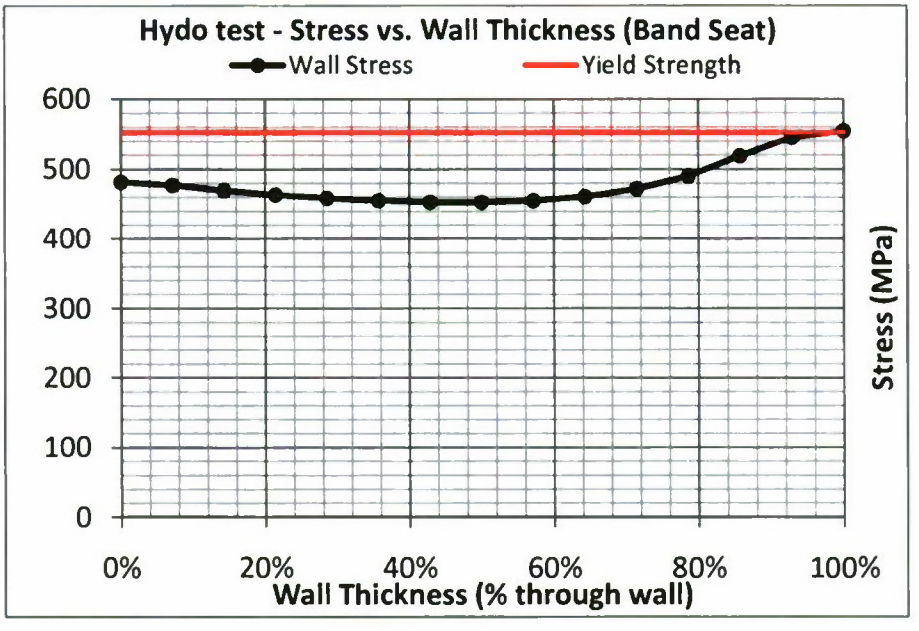


Figure 22
von Mises stress at band seat during hydrostatic testing

Critical Flaw Size (Method, Damage Tolerant Design)

In damage tolerant design, the engineer assumes 1) that a flaw smaller than a critical size may be present and 2) the munition should operate safely and reliably with the flaw present. The rate of flaws being present is relatively low. In a recent mortar projectile sorting, for instance, 100% of 24,300 mortar bodies were x-rayed for defects. Fifty-nine parts had defects. All defects were smaller than the critical size (ref. 4).

Critical flaw sizes for the 81-mm mortar were estimated using the linear elastic fracture mechanics assumptions. Even with 10% blow-by added to the mortar shell, very little plasticity resulted. This is consistent with the linear elastic fracture assumption. The critical flaws estimates were completed after the stress analysis. Flaws were estimated for the hydrostatic test and for the gun launch loads.

Hydrostatic test - the hydrostatic test result placed the defect area in figures 1 and 2 in tension. The following steps were completed for the critical flaw analysis:

1. Complete ABAQUS dynamic analyses as described.

2. From the dynamic load sequence, the maximum stress distribution was used for predicting the critical flaw size. ABAQUS version 6.9.1 (ref. 2) has a filter option that records the maximum stress over all of the dynamic time steps.

3. In the region of the flaw (figs. 1 and 2), the hydro test resulted in tension stress in the hoop direction. Figure 13 shows the hoop stress distribution through the wall thickness. The stress distribution is slightly nonlinear and in tension through the wall.

4. Using the stress distribution from the ABAQUS output, the critical defect was calculated using the NASGRO software package. The mortar was roughly a cylinder. The three NASGRO defect cases (fig. 14) were used to estimate the flaw. In previous Army studies, these cases were validated by comparison to classical solutions (refs. 6 and 7).

5. For instance, case SC04 can be used to determine the size of an internal defect in a cylinder. Input data includes wall thickness at the point of interest, wall outer diameter, and normalized stress distribution. The normalized stress distribution (fig. 13) can be cut and pasted from an Excel spread sheet into NASGRO. The fracture toughness was assumed to be 21-MPa$\sqrt{m}$ (ref. 4) for the HF-1 material. The starting point for the estimated flaw size was chosen as a relatively small number, 0.001. The calculation was completed assuming a maximum $K_I$ value for either the a-tip or the c-tip. Crack ratios, a/c, of 0.1 and 1.0 were used. A ratio of 0.1 represents a scratch.

6. Similar analyses were completed with the axial stresses for the two load cases.

7. The critical flaw size for the hydrostatic case and the gun launch case was greater than one fourth through the wall thickness. The specified flaw reverted to the one fourth of wall thickness as originally specified.

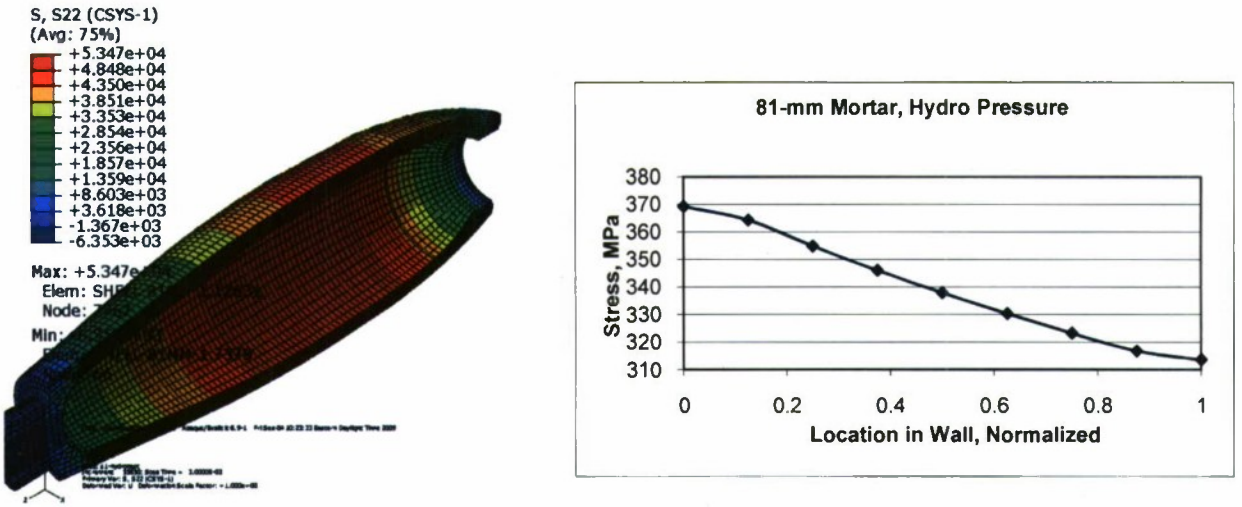


Figure 23
Hoop stress near flaw from hydrostatic test

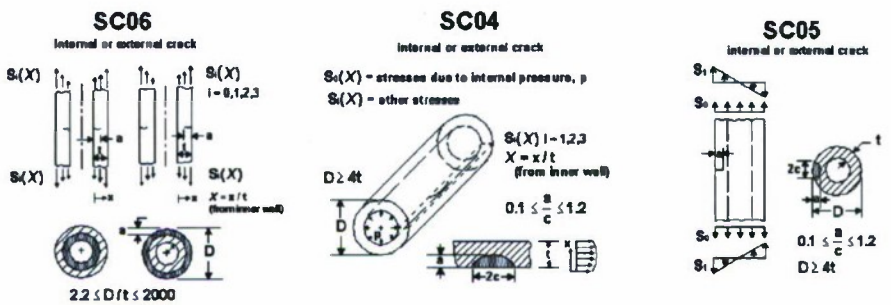


Figure 24
NASGRO (ref. 3) surface crack orientations for cylinders

## DISCUSSION

The analysis indicated that defects similar to the ones observed are not likely to cause a catastrophic failure. However, a shell body containing such flaws is inadequate to be fielded and should be discarded. Since the fracture toughness was assumed to be 21.0 MPa$\sqrt{m}$, it is recommended that screening be performed to verify that the actual fracture toughness of the M821A1 shells is greater than the assumed value. It is important to note that simplified flaw geometry was assumed in determining the critical flaw size, but the pitting that was observed in the shell body was much more complex in its structure. As such, there is uncertainty in the behavior of a defective round being fired, assuming its flaw geometry is outside of the scope of the fracture model used. This fact, in-part, contributes to the recommendation to reject parts with this defect.

## CONCLUSIONS

A finite element analysis of an 81-mm M821A1 assembly was completed to calculate stress distributions for various loading cases, which included hydro testing and gun launch conditions. When flaws of up to one third the wall thickness on the interior surface of the M821A1 shell body and up to one fourth the wall thickness on the interior of the shell body are incorporated (reflecting actual observations), the stress distributions indicate that the part will not fail during hydro testing or gun launch, although yielding may occur in some load cases. The results of each of these load and flaw cases are summarized in the following table. The 60-mm pressure-time curve represents a conservative upper bound load case for the M821A1 mortar, whereas, the 81-mm pressure-time curve is more representative of actual fielding conditions. Despite some yielding of the shell body, the results indicate that the 81-mm M821A1 mortar will not catastrophically fail with the incorporated defects. Regardless, the recommended critical flaw size is one fourth the wall as a thickness. It is suggested that this result is used for critical flaw depth criterion and that any additional parts with the same observed defect size (or larger) be discarded.

Maximum stress to yield strength ratio for various load cases

| Load case | Interior flaw | Internal flaw |
|---|---|---|
| Hydrostatic test | 100.9 % | 64.3 % |
| Gun launch (overpressure) | 104.5 % | N/A |
| Gun launch (81-mm pressure-time curve) | 72.1 % | 48.9 % |

## REFERENCES


1. Hespos, M., "Metallurgical Evaluation of 81-mm Mortar Body Defect," Internal Report, U.S. Army Armament Research, Development and Engineering Center, Picatinny Arsenal, NJ, 2009.

2. Abaqus Inc., "Abaqus User Manual V6.91," 2008.

3. NASGRO, Version 5.0, Swri Main Office, 6220 Culebra Road, P.O. Drawer 28510, San Antonio, Texas, 2006.

4. Cordes, J.A.; Thomas, J.; Wong, R.S.; and Carlucci, D., "Reliability Estimates For Flawed Mortar Projectile Bodies," Reliability, Engineering & System Safety, Volume 94, Issue 12, pages 1887-1893, 2009

5. Cordes, J.A.; Carlucci, D.E.; Kalinowski, J.; and Reinhardt, L., "Design and Development of Reliability Gun-Fired Structures," Technical Report ARAET-TR -06009, U.S. Army Armament Research Development and Engineering Center, Picatinny Arsenal, NJ, 2006.

6. Anderson, T.L., Fracture Mechanics, Fundamentals and Applications, CRC Press, Inc, Boca Raton, Fl, 2nd Edition, pp. 627-636, 1995.

7. Barsom, J.M. and Rolfe, S.T., Fracture & Fatigue Control In Structures, 2nd Edition, Prentice-Hall, Englewood Cliffs, NJ, 1987.

## DISTRIBUTION LIST

U.S.Army ARDEC
ATTN: RDAR-EMK
RDAR-GC
RDAR-MEF, W. Smith
RDAR-ME, J. Hedderich
RDAR-MEF-E, J. Jablonski (10)
Picatinny Arsenal, NJ 07806-5000

Defense Technical Information Center (DTIC)
ATTN: Accessions Division
8725 John J. Kingman Road, Ste 0944
Fort Belvoir, VA 22060-6218

Commander
Soldier and Biological/Chemical Command
ATTN: AMSSB-CII, Library
Aberdeen Proving Ground, MD 21010-5423

Director
U.S. Army Research Laboratory
ATTN: AMSRL-CI-LP, Technical Library
Bldg 4600
Aberdeen Proving Ground, MD 21005-5066

Chief
Benet Weapons Laboratory, CCAC
Armament Research, Development and Engineering Center
U.S. Army Research, Development and Engineering Command
ATTN: AMSRD-AAR-AEW
Watervliet, NY 12189-5000

Director
U.S. Army TRADOC Analysis Center-WSMR
ATTN: ATRC-WSS-R
White Sands Missile Range, NM 88002

Chemical Propulsion Information Agency
ATTN: Accessions
10630 Little Patuxent Parkway, Suite 202
Columbia, MD 21044-3204

GIDEP Operations Center
P.O. Box 8000
Corona, CA 91718-8000